

Journal of Biomedical Optics

BiomedicalOptics.SPIEDigitalLibrary.org

Polarization dependence of aligned collagen tissues imaged with second harmonic generation microscopy

Francisco J. Ávila
Oscar del Barco
Juan M. Bueno

Polarization dependence of aligned collagen tissues imaged with second harmonic generation microscopy

Francisco J. Ávila, Oscar del Barco, and Juan M. Bueno*

Universidad de Murcia, Instituto Universitario de Investigación en Óptica y Nanofísica, Laboratorio de Óptica, Campus de Espinardo (Ed. 34), Murcia 30100, Spain

Abstract. A polarimetric second harmonic generation (SHG) microscope was used to analyze the dependence between polarization and SHG signal from collagen-based samples. A theoretical model was also developed to investigate the SHG intensity as a function of different polarization states for a set of quasiparallel fibers. Numerical simulations were compared to experimental SHG intensity values and a fairly good agreement was found. Linear polarized light produced periodical changes in the emitted SHG signal with a maximum of intensity corresponding to polarization parallel to the main orientation of the fibers, regardless the ratio of hyperpolarizabilities, ρ . A similar behavior was found for elliptical states located along a vertical meridian on the Poincaré sphere (i.e., null azimuth) although the modulation of the SHG signal was different. Our numerical calculations described a dramatic change in this regular trend when ρ changed from positive to negative values. Moreover, we provide an experimental method (based on the analysis of the modulation of the SHG signal) to determine the value of the ratio ρ and, consequently, to obtain information about the internal organization of the collagen fibers. © 2015 Society of Photo-Optical Instrumentation Engineers (SPIE) [DOI: 10.1117/1.JBO.20.8.086001]

Keywords: polarization; second harmonic generation; nonlinear microscopy; collagen.

Paper 150043RRR received Jan. 26, 2015; accepted for publication Jun. 30, 2015; published online Aug. 11, 2015.

1 Introduction

Collagen is the most abundant structural protein in the human body. There are more than 20 classified types, all characterized by a triple helical domain.¹ In particular, type-I collagen consists of nanometer-scale fibrils assembled in micrometer-scale bundles or fibers and can be found in a wide variety of tissues such as skin, dentine, cornea, sclera, bone or tendon. Fibrils within a fiber could be arranged parallel to each other, or present random or interlaced patterns.²⁻⁴ Moreover, collagen fibers might also exhibit both organized and disorganized arrangements.^{5,6}

Second harmonic generation (SHG) imaging is a nonlinear microscopy technique where, in the absence of absorption, two photons interact with a noncentrosymmetrical structure. As a result, light at exactly half of the excitation wavelength is emitted.^{7,8} An SHG signal can be generated by biological tissues containing microtubules, myosin and collagen;^{9,10} the latter is an excellent SHG emitter due to its significant second-order nonlinear susceptibility.¹¹ SHG has been proved to be a useful tool to analyze abnormal or pathological tissues,^{12,13} and to explore changes after surgical procedures^{14,15} among others.

The intensity of these nonlinear signals is not only a function of the collagen content but it is also modulated by the collagen organization. Moreover, polarization-dependent measurements of biological tissues help in the analysis of the optical anisotropy of the samples. In particular, SHG is sensitive to the polarization of the incident beam and provides valuable information related to the structure and type of the collagen

fibers^{16,17} and molecular organization.¹⁸ Nowadays, it is well-known that the polarization-sensitivity of the SHG signal can be characterized by the ratio of the first-order hyperpolarizabilities, ρ .^{16,19} This ratio, defined as $\rho = \beta_{xxx}/\beta_{yyy}$, is related to the internal collagen spatial distribution. This parameter has been reported to vary in the range $[-3, 3]$.²⁰⁻²² In tendons, immature collagen fibrils present low ρ values.²⁰ Moreover, there is also a decrease in ρ associated with collagen aging (as reported in Refs. 10, 23, 24).

Most experiments combined linear polarized light and SHG imaging to visualize features in collagen-based samples.^{10,16,25} Some authors reported theoretical models and/or experimental measurements to characterize the response of the SHG signal from collagen fibers to linear^{10,19,21} and elliptical polarized light.²⁶ Recently, a theoretical model has also analyzed the role of elliptical polarized light in the SHG signal produced by a single collagen fiber.²⁷ In this sense, polarization-sensitive SHG microscopy has been used as an effective technique to analyze the hierarchical architecture of collagen^{28,29} and has gained popularity due to its potential to discriminate normal collagen tissues from diseased ones.³⁰⁻³²

The aim of this work is to further analyze the SHG signal from a set of elongated collagen fibers for incident linear and elliptical polarized light. To better understand the effects of polarization on SHG microscopy, experimental images of collagen structures lying along a dominant direction have been recorded and compared to a numerical model. Moreover, we provide an experimental method (based on the analysis of the modulation of the SHG signal) to determine the value of the

*Address all correspondence to: Juan M. Bueno, E-mail: bueno@um.es

ratio ρ and, consequently, to obtain information about the internal organization of the fibrils within the collagen fibers.

2 Methods

2.1 Theoretical Model: General Expression for the Intensity of a Second Harmonic Generation Signal

Let us consider an elliptically polarized light (azimuth χ and ellipticity ψ), with fundamental frequency ω , and propagating along the \hat{Z} direction. The beam is focusing on a set of collagen fibers through a microscope objective with numerical aperture $\text{NA} = n_\omega \cdot \sin \Theta$ (see Fig. 1) where Θ corresponds to the maximum angle at which the light rays reach the sample and n_ω represents the index of refraction of collagen. The components of the polarization ellipse referred to the Cartesian coordinate system (\hat{X}, \hat{Y}) can be written as²⁷

$$E_{\omega,X}(x, y, z) = -iE_{\omega,X}^{(0)} \exp\left[-\left(\frac{x^2 + y^2}{w_{xy}^2} + \frac{z^2}{w_z^2}\right)\right] \exp[i\xi k_\omega z], \quad (1)$$

$$E_{\omega,Y}(x, y, z) = -iE_{\omega,Y}^{(0)} \exp\left[-\left(\frac{x^2 + y^2}{w_{xy}^2} + \frac{z^2}{w_z^2}\right)\right] \exp[i\xi k_\omega z + \delta], \quad (2)$$

where $k_\omega = 2\pi n_\omega / \lambda_\omega$ is the corresponding wave number, λ_ω corresponds to the wavelength of the incident polarized light, and δ is the phase difference between these two orthogonal components. ξ stands for a wave-vector reduction factor that characterizes the phase shift experienced by a Gaussian beam in the vicinity of a focal center, and w_{xy} and w_z represent the $1/e$ radii of the focal ellipse in the lateral and axial directions³³

$$w_{xy} = \frac{0.32\lambda_\omega}{n_\omega \sin \Theta} \quad w_z = \frac{0.53\lambda_\omega}{n_\omega (1 - \cos \Theta)}. \quad (3)$$

For a single collagen fiber, the incident electrical field induces an SHG signal $E_{2\omega}$ [see the Appendix for a detailed deduction of the SHG intensity $I_{2\omega}$, Eq. (19)] which depends on the SHG emission direction (θ, φ) (see Fig. 1), the incident wavelength λ_ω , the numerical aperture NA, the incident polarization (azimuth χ and ellipticity ψ), and the ratio of hyperpolarizabilities ρ . This ratio is related to the internal collagen organization^{30,21} and plays a fundamental role in our model.

Nevertheless, the sample here considered is composed of N collagen fibers arranged in a “quasiparallel” distribution (that is, they are lying mainly along the \hat{x} direction). In order to include this external organization in our model, a maximum dispersion of $\Delta x = \pm 20$ deg among collagen fibers has been allowed. Moreover, a random variation of the ratio ρ about a mean value, in consistency (as explained later in Sec. 3.2) with the standard deviation of our experimental data, has also been performed.

Taking this into account, the total SHG intensity $\tilde{I}_{2\omega}$ can be numerically computed as the incoherent sum of N intensity values $I_{2\omega,j}$ from each “quasialigned” collagen fiber as

$$\tilde{I}_{2\omega} \approx \sum_{j=1}^N I_{2\omega,j}^{\alpha_j}, \quad (4)$$

where α_j stands for the angle between a collagen fiber and the \hat{x} direction (randomly varying between 0 and ± 20 deg).

The total SHG intensity was computed in the backscattered direction (B-SHG; $\pi/2 < \theta < 3\pi/2$) for different polarization states, via Eq. (4). For the sake of simplicity, the first factor in Eq. (19) was normalized to unity.²⁷

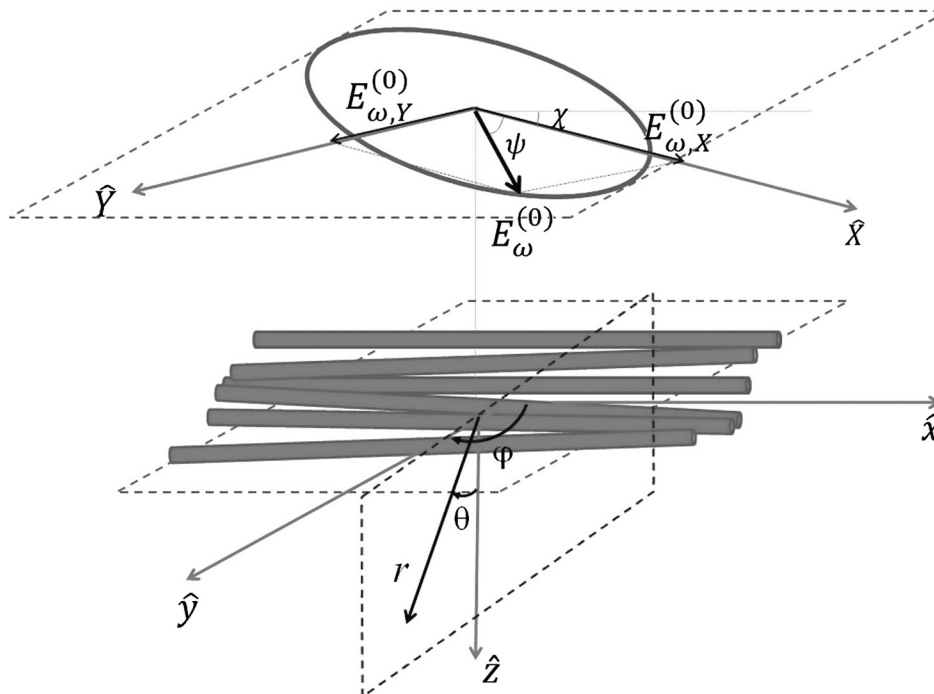


Fig. 1 A beam of elliptically polarized light propagating along the \hat{Z} direction focusing on a set of N collagen fibers mainly aligned along the \hat{x} axis.

The incident polarization states in our model were the same as those used in the experimental configuration (see details below): linear and elliptical. Linear polarization states $S_{2\psi=0}$ (null ellipticity, $2\psi = 0$) are on the equatorial plane of the Poincaré sphere. Elliptical polarization states $S_{2\chi=0}$ were chosen to be located along a single vertical meridian with null azimuth ($2\chi = 0$). In terms of the Stokes vector, these linear and elliptical states used here can, respectively, be expressed as³⁴

$$S_{2\psi=0} = \begin{pmatrix} 1 \\ \cos(2\chi) \\ \sin(2\chi) \\ 0 \end{pmatrix} \quad S_{2\chi=0} = \begin{pmatrix} 1 \\ \cos(2\psi) \\ 0 \\ \sin(2\psi) \end{pmatrix}. \quad (5)$$

2.2 Experimental System: Polarization-Sensitive Multiphoton Microscope

Figure 2 shows a simplified diagram of the custom multiphoton microscope.⁵ In brief, a mode-locked Ti:Sapphire laser used as illumination source (λ_w set at 760 nm) was coupled into an inverted microscope. After reflection in a dichroic mirror, the beam reached the sample through a nonimmersion microscope objective (NA = 0.5). Nonlinear signals from the samples were detected in the backward direction via the same microscope objective. The B-SHG signal from the collagen-based structures was isolated via a narrowband (380 ± 10 nm) spectral filter placed in front of the photomultiplier tube used as a recording unit. Images were scanned by a device formed by a pair of non-resonant galvanometric mirrors.

A polarization state generator (PSG) was placed across the illumination pathway to modulate the polarization state of the incident light. This PSG was composed of a fixed horizontal

linear polarizer (P_L), a rotatory half-wave plate ($\lambda/2$) and a removable quarter-wave plate ($\lambda/4$) (see Fig. 3). This configuration allows the generation of two sets of polarization states, as follows. When $\lambda/4$ is removed [Fig. 3(a)], the rotation of the $\lambda/2$ produced linear polarization states covering the equatorial plane of the Poincaré sphere. As is well-known, the effect of a $\lambda/4$ is to rotate the incident Stokes vector at an angle of 90 deg around its fast axis in the counter-clockwise direction. Then when the $\lambda/4$ was introduced into the system with its fast axis at the vertical and horizontal positions, the linear states emerging from the $\lambda/2$ turned into elliptical polarization states with null azimuth [$2\chi = 0$, Fig. 3(b)].

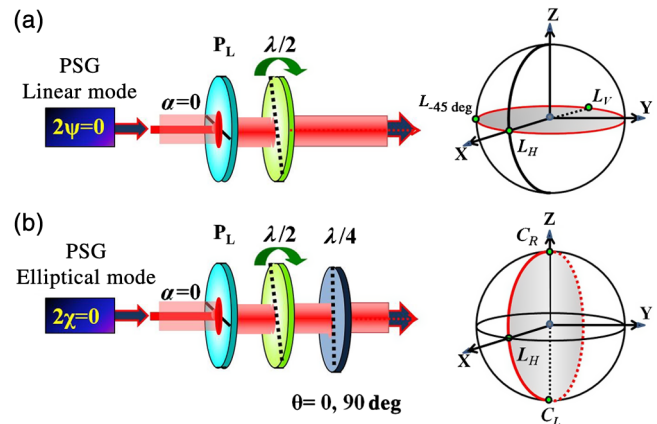


Fig. 3 Experimental configuration of the PSG. P_L , linear polarizer; $\lambda/2$, rotatory half-wave plate, and $\lambda/4$, removable quarter-wave plate. The Poincaré spheres on the right show the two sets of polarization states: one placed in the (a) equatorial plane and the other in the (b) vertical meridian.

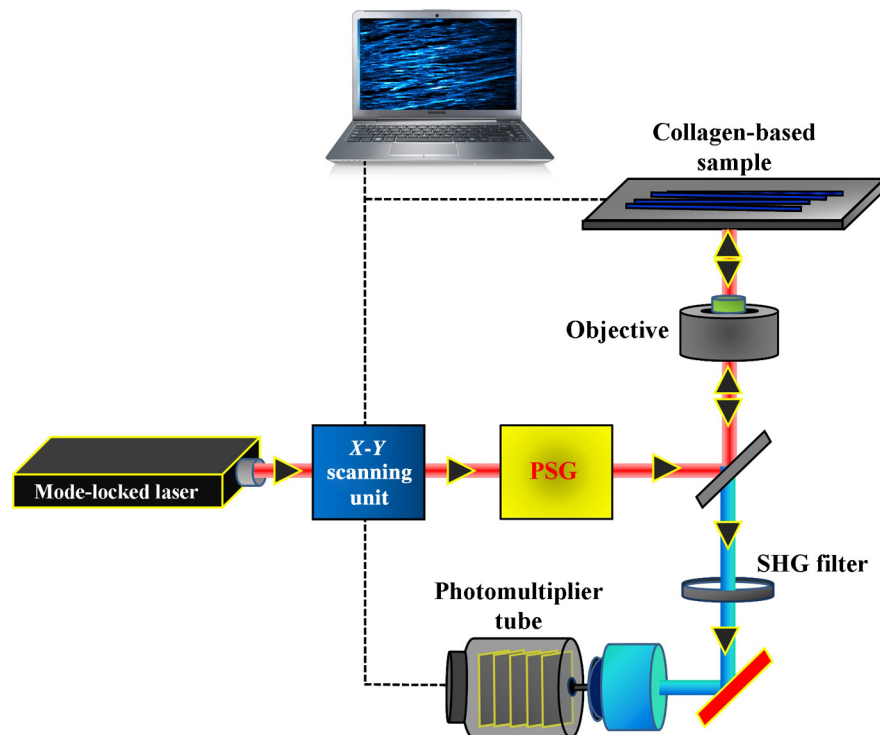


Fig. 2 Schematic diagram of the multiphoton microscope used to record second harmonic generation (SHG) images of collagen-based samples. PSG, polarization state generator.

The reflection of a light beam on a dichroic mirror modifies the ellipticity of the polarization states produced by the PSG.³⁵ This optical element could also present diattenuation,³⁶ which means that the amount of reflected light might depend on the incident polarization state. First, the dependence of the reflected light with the incident polarization states was tested. This showed variations smaller than 1.5%. Changes in ellipticity were also analyzed for all polarization states used in this work. Toward this aim, an analyzer unit ($\lambda/4$ + linear polarizer) was inserted in the forward direction

as previously reported.³⁷ Results showed differences lower than 5% between the nominal and the measured polarization states.

2.3 Experimental Second Harmonic Generation Imaging

Polarimetric SHG images for samples of ocular tissues composed of type-I collagen were recorded in the backscattered direction. This configuration would be more suitable for future *in vivo* experiments. In particular, the tissues were nonstained histological transversal sections of human sclera (sample #1) and rabbit cornea (sample #2). These arrangements presented a well-organized collagen distribution with their fibers lying mainly along the \hat{x} axis. As an example, Fig. 4 shows experimentally recorded SHG images corresponding to those collagen-based ocular tissues, acquired for different polarization states produced in the PSG. These images corresponded to planes located at $\sim 5\text{-}\mu\text{m}$ depth. Since wavelength and depth location within the samples were constant, changes in the hyperpolarizability and SHG signal with wavelength or tissue depth did not occur.³⁸

For the first configuration ($P_L + \lambda/2$), the $\lambda/2$ was rotated to produce linear polarized states 15 deg apart in azimuth. Elliptical and circular states placed in the vertical meridian of the Poincaré sphere were also generated by the second configuration ($P_L + \lambda/2 + \lambda/4$) in steps of 15 deg.

A previous image processing procedure, involving a parameter known as structure tensor^{39,40} allowed us to estimate the actual fiber directional dispersion (Δx) of these samples. Although those tests are out of the scope of this work, the data provided

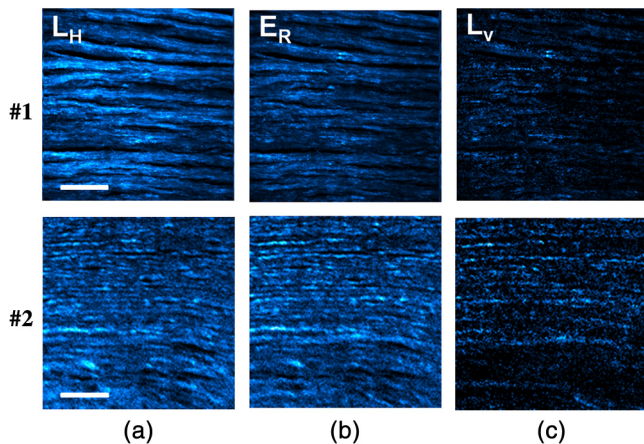


Fig. 4 Experimental SHG images for two different collagen structures as a function of the incident polarization state: (a) L_H , linear horizontal; (b) E_R , elliptical; and (c) L_V , linear vertical. Scale bar: 50 μm .

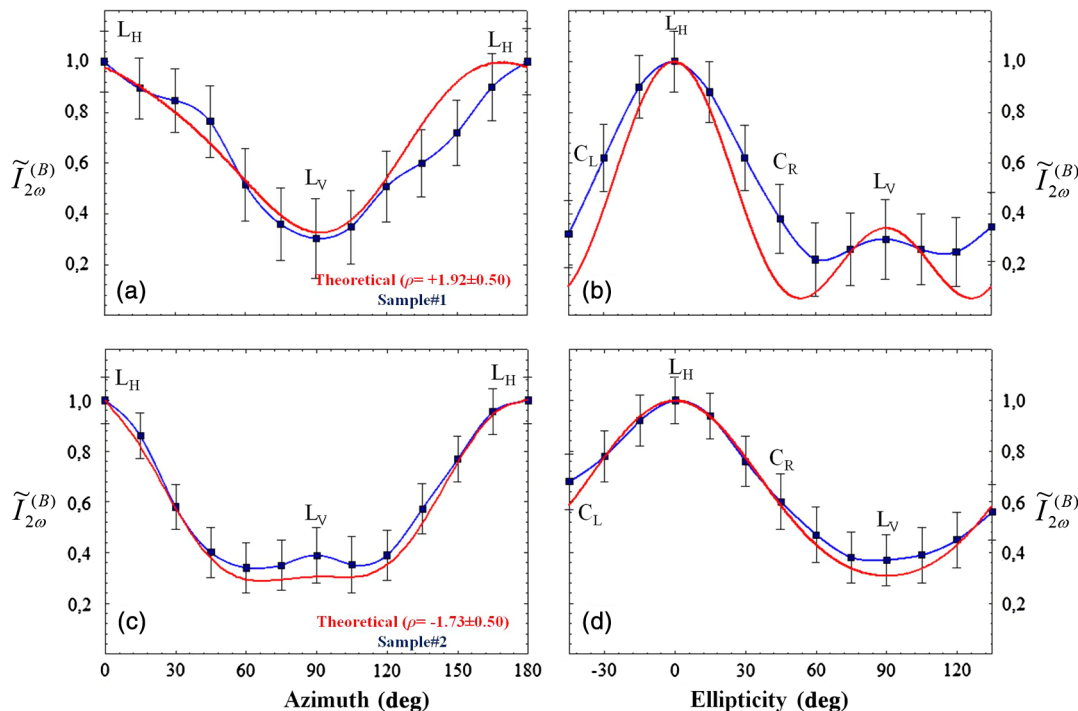


Fig. 5 Theoretical ($\rho = +1.92$ and -1.73) and experimental B-SHG intensity curves as a function of the (a), (c) azimuth and the (b), (d) ellipticity of the incident light. Numerical simulations were computed for $N = 30$ and $\Delta x = \pm 20$ deg. Experimental results correspond to the two collagen-based samples (Fig. 4) containing fibers lying mainly along the \hat{x} axis. L_H , L_V , C_R , and C_L indicate linear horizontal, linear vertical, right circular, and left circular polarized lights, respectively.

are of great importance to compare the experimental results and the theoretical model. For the samples here used, Δx values were ± 13 deg (sample #1) and ± 17 deg (sample #2). The imaged area corresponded to an area of $210 \times 210 \mu\text{m}^2$ and every final image was averaged over three individual frames (250×250 pixels). Image processing was performed through home-made MATLAB® software.

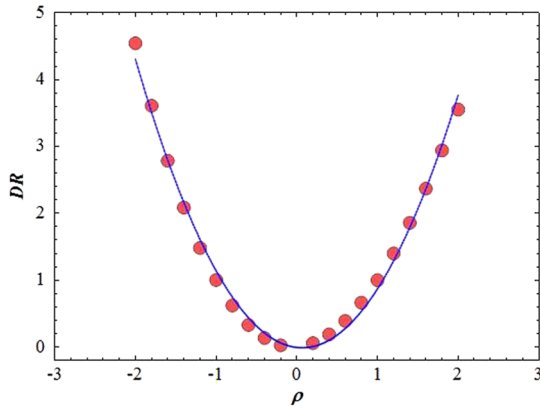


Fig. 6 Numerical calculations of the dichroic ratio (DR), as a function of the parameter ρ ($N = 30$ and $\Delta x = \pm 20$ deg). The line corresponds to the best fit (parabolic curve).

3 Results

3.1 Second Harmonic Generation Signal from Collagen as a Function of the Incident Polarization

Figure 5 compares theoretical and experimental results for B-SHG intensity values, $\tilde{I}_{2\omega}^{(B)}$ as a function of the azimuth (left plots) and the ellipticity (right plots) of the incident light. The former were computed for a set of 30 collagen fibers with a directional dispersion $\Delta x = \pm 20$ deg and two different values of ρ , $+1.92$ (upper plots) and -1.73 (bottom plots) with the corresponding variability ($\rho \pm 0.5$, for the samples here involved). These values were computed as described in the next Sec. 3.2. The latter corresponded to the total B-SHG intensity computed from images of samples #1 and #2 shown in Fig. 4. Data have been normalized to their maximum for a better comparison.

A visual inspection reveals a similar behavior of the $\tilde{I}_{2\omega}^{(B)}$ between theoretical and experimental results. Moreover, statistical analyses (t -test) do not show significant differences ($p > 0.15$ for all them). In particular, Figs. 5(a) and 5(c) depict the relationship between $\tilde{I}_{2\omega}^{(B)}$ and the incident linear polarized light. These two plots show that the B-SHG signal changes periodically with the azimuth χ , presenting a maximum signal when the incident linear state is parallel to the collagen fiber (L_H) and a minimum value for the orthogonal direction (where $\rho > 0$).

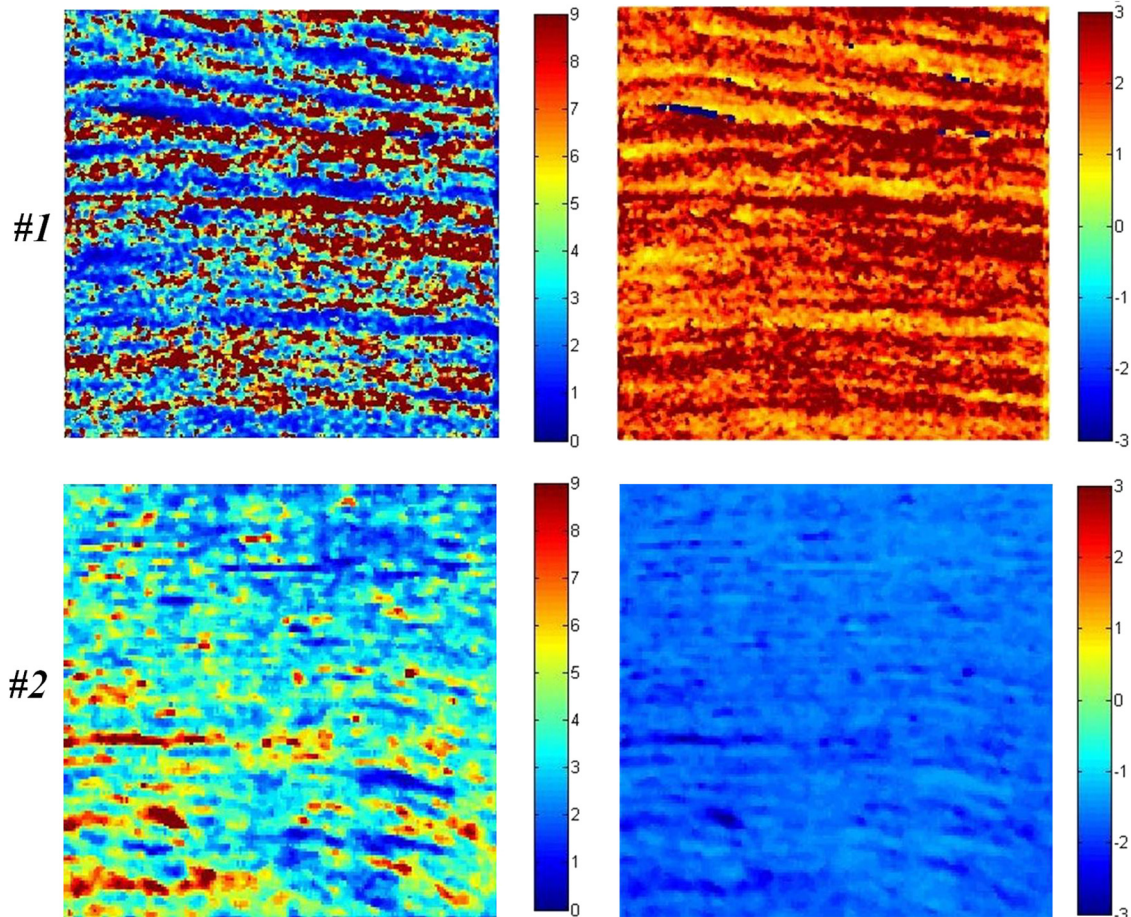


Fig. 7 Spatially resolved maps of (a) DR and (b) ρ for samples #1 and #2.

On the other hand, when the incident polarization covers the vertical meridian with null azimuth on the Poincaré sphere (see Fig. 3), the behavior of the B-SHG signal changes dramatically [as shown in Figs. 5(b) and 5(d)]. As expected, the B-SHG intensity reaches a maximum for L_H and decreases as we move along the vertical meridian on the Poincaré sphere. Elliptical polarized light yields a higher modulation than linear polarization for positive values of ρ [see Fig. 5(b)].

For sample #1 (with $\rho > 0$), a minimum for L_V appears [Fig. 5(a)] for the set of linear states. However L_V provides a secondary maximum in the case of the elliptically polarized light [Fig. 5(b)]. The behavior of the curve with elliptical incident light for sample #2 (with $\rho < 0$) is clearly different [Fig. 5(d)] and L_V is associated with a minimum B-SHG intensity value.

3.2 Experimental Calculation of the Parameter ρ

As previously stated, the ratio of hyperpolarizabilities, ρ , provides information about the internal organization of the fibrils within the fibers. In this section, we propose an experimental method to compute this parameter via the “dichroic ratio” (DR), defined as the ratio of the intensities for linear horizontal (L_H) and vertical (L_V) polarized light ($DR = I_H/I_V$).⁴¹ Figure 6 depicts the DR numerically computed for different values of ρ , in a set of 30 collagen fibers and directional dispersion $\Delta x = \pm 20$ deg. These theoretical data can be fitted to a parabolic curve, that is, $DR = 0.81\rho^2 - 0.15\rho + 0.22$ ($R^2 = 0.99$, $p < 0.0001$).

However, this DR yields the modulus of ρ , but not the sign. In order to obtain the sign of ρ , extra information is required. This can be directly extracted from the shape of the B-SHG curve for elliptical polarized states (compare top and bottom plots in Fig. 5). At this point the question would be: Is it necessary to perform a large set of polarization states to completely determine the parameter ρ (i.e., sign and modulus)? The answer to this question is “no.” In particular, for a complete determination of ρ , only three experimental values of the SHG intensity are required. These correspond to three linear polarization states: L_H , L_V , and linear with $\chi = 60$ deg or 120 deg (L_{60} or L_{120}).

In this sense, L_H and L_V are used to compute the modulus of ρ , and L_{60} will provide the sign as follows (see Fig. 5): ρ will be positive if $\tilde{I}_{2\omega}^{(B)}$ for L_V is lower than $\tilde{I}_{2\omega}^{(B)}$ for L_{60} . Otherwise, ρ will be negative.

In this sense, for each sample the point-by-point DR can be computed from the relationship between the B-SHG signal and the corresponding incident polarization states. Therefore, taking into account the above information, the ratio ρ can be easily derived. Figure 7 depicts the spatially resolved maps for DR (a) and ρ (b) for samples #1 and #2. The experimentally-derived values of the ratio ρ across the entire images were $\rho = +1.92 \pm 0.50$ and $\rho = -1.73 \pm 0.60$, respectively.

Finally, in order to check if these experimental values of ρ are coherent with our numerical model, Fig. 8 compares numerical and experimental B-SHG intensities values as a function of the incident linear polarization. A polar representation has been chosen for a better visualization and direct comparison. It can be noticed that there is good agreement between both sets of data, what corroborates the fairly good accuracy in the experimental calculation of the ratio ρ (t-test indicates that differences were not significant).

4 Discussion and Conclusions

We developed a theoretical model to analyze the dependence between the B-SHG intensity and the incident polarization, in sets of elongated collagen fibers. Linear and elliptical polarized states have been considered. The analytical expression for the B-SHG signal depended on the azimuth (χ) and the ellipticity (ψ) of the incoming polarized light, the ratio of hyperpolarizabilities (ρ) and the collagen fiber dispersion (Δx). The B-SHG signals have been numerically computed for the same objective NA and incident wavelength λ_ω values as those considered in real measurements.

Theoretical data have been compared to experimental results obtained from SHG images of collagen-based tissues recorded with a multiphoton microscope. A set of N collagen fibers arranged in a “quasiparallel” distribution was considered for the numerical simulation. The samples involved in the study were ocular tissues composed of collagen fibers mainly aligned along the \hat{x} direction.

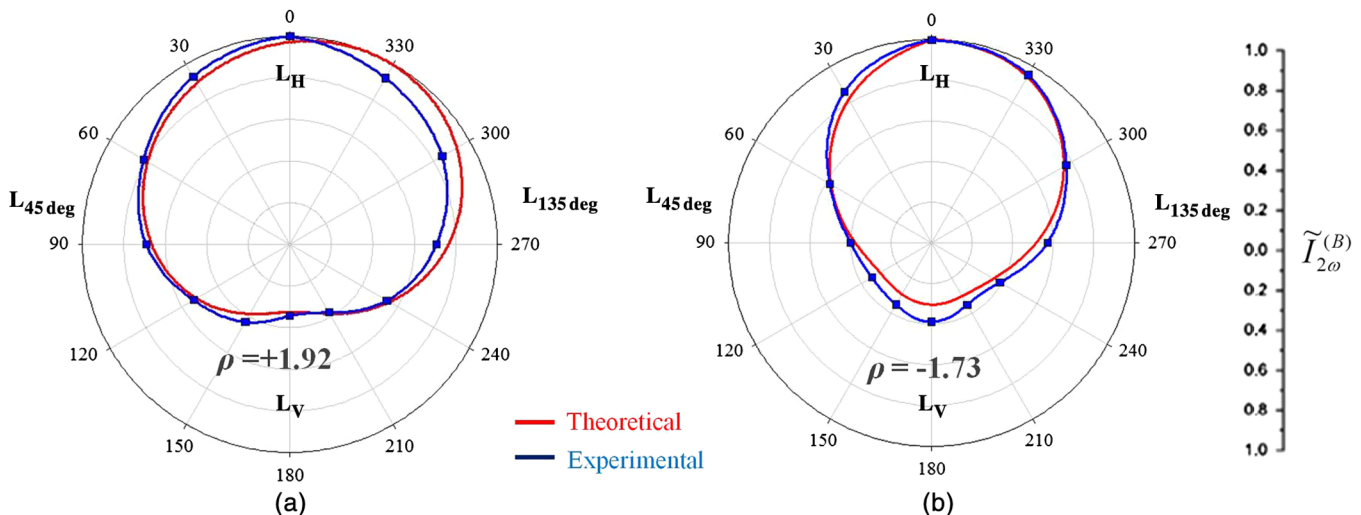


Fig. 8 Comparison of theoretical and experimental data of B-SHG intensity values for incident linear polarized light. Plots correspond to sample (a) #1 and (b) #2. As indicated, numerical simulations were carried out for two values of ρ (+1.92 and -1.73).

Theoretical results showed a periodic B-SHG intensity distribution for incoming linear polarized states [Figs. 5(a) and 5(c)], with a maximum for horizontal polarization, that is, parallel to the single collagen fiber. Vertical polarized light provided a (non-null) minimum. B-SHG experimental values for both samples agreed with theoretical calculations.

For elliptical polarized light located along a vertical meridian with a null azimuth, numerical calculations showed a maximum for a linear horizontal light and a secondary maximum for linear vertical states when ρ was positive [Fig. 5(b)]. Experimental results presented similar trends.

When $\rho < 0$, both sets of data were also in fairly good agreement [Figs. 5(c) and 5(d)]. These corroborate previous theoretical work reported for linear²¹ and elliptical polarized light.²⁷ Here, we have further explored numerical calculation and experimental data in the backscattered direction. Moreover, the differences in the behavior of the B-SHG signal when ρ is positive or negative were clearly stated and are coherent with the model. It is also interesting to notice how the shape of the curve for elliptical light gives information about the sign of ρ .

It has been reported that the SHG intensity is maximum for an excitation wavelength around 800 nm,^{38,42} therefore, lower values of λ_ω could yield deviations of Kleinman's symmetry. In this work, we have used 760 nm and Kleinman's symmetry could not be rigorously applied. Despite this, our model represents a reasonable good approximation.

On the other hand, the parameter ρ depends on the orientation of the nonlinear dipoles within the collagen triple helices and provides information about the ordering of collagen molecules or fibrils within the focal volume. The usual method is to measure the ratio ρ of the two main tensorial components of the nonlinear response, considering a cylindrical symmetry for fibrillar collagen.^{10,43} Gusachenko et al.¹⁹ reported a reliable determination of ρ accounting for the effects of both diattenuation and birefringence.

Based on the computation of the DR, an approach to experimentally determine the value of the ρ has been developed here. Spatially-revolved maps of ρ are shown for the samples involved in the study. The experimental ρ values have been compared with the numerical simulation corresponding to those values. Results agree well (see Fig. 8), which provides a reliable method to determine the parameter ρ .

In conclusion, we combined numerical modeling and experiments in collagen-aligned samples to investigate the dependence between the incident polarization and the B-SHG intensity. We evidenced that polarization noticeable modulates this nonlinear signal originated in collagen-based structures; however, the response strongly depends not only on the set of polarization states but also on the internal structure of the imaged sample. From the B-SHG signal modulation we derived an easy method to process the value of ρ (both modulus and sign). Further analyses in nonorganized collagen samples will give insight into the general dependence between polarization and the originated SHG signal. Since pathological processes tend to alter the original collagen organization, the accurate measurement of ρ will be important to discriminate healthy from pathological tissues and might help to provide future implementations of polarimetric SHG imaging into clinical applications.

Acknowledgments

This work has been supported by the SEIDI, Spain, grant FIS2013-41237-R and EU FEDER funds.

Appendix: Second Harmonic Generation Intensity for a Single Collagen Fiber

The total dipole moment $\vec{\mu}$ induced by the incident field \vec{E}_ω can be expressed as²⁵

$$\vec{\mu} = \vec{\mu}_0 + \alpha \cdot \vec{E}_\omega + \frac{1}{2!} \beta \cdot \vec{E}_\omega^2 + \frac{1}{3!} \gamma \cdot \vec{E}_\omega^3, \quad (6)$$

where μ_0 is the permanent dipole moment and α , β , and γ correspond to the linear polarizability and first and second hyperpolarizabilities, respectively. The electric dipole moment associated to the SHG signal is related to the third term.⁴⁴

On the basis of the definition of the second-order tensor, hyperpolarizabilities owns 27 items. Nevertheless, under cylindrical and Kleinman symmetries^{45,46} the hyperpolarizability tensor can be further simplified and reduces to two terms, namely β_{xxx} and β_{xyy} . Therefore, the dipole moment induced by the incident electric field $E_{\omega,X}$ can be written as⁴⁴

$$\begin{aligned} \mu_{2\omega,x}^{(X)}(x, y, z) &= \frac{1}{2} E_{\omega,X}^2 (\beta_{xxx} \cos^2 \chi + \beta_{xyy} \sin^2 \chi), \\ \mu_{2\omega,y}^{(X)}(x, y, z) &= \frac{1}{2} E_{\omega,X}^2 \beta_{xyy} \sin(2\chi), \\ \mu_{2\omega,z}^{(X)}(x, y, z) &= 0, \end{aligned} \quad (7)$$

and for the dipole moment induced by $E_{\omega,Y}$

$$\begin{aligned} \mu_{2\omega,x}^{(Y)}(x, y, z) &= \frac{1}{2} E_{\omega,Y}^2 \left[\beta_{xxx} \cos^2 \left(\chi + \frac{\pi}{2} \right) + \beta_{xyy} \sin^2 \left(\chi + \frac{\pi}{2} \right) \right], \\ \mu_{2\omega,y}^{(Y)}(x, y, z) &= \frac{1}{2} E_{\omega,Y}^2 \beta_{xyy} \sin \left[2 \left(\chi + \frac{\pi}{2} \right) \right], \\ \mu_{2\omega,z}^{(Y)}(x, y, z) &= 0. \end{aligned} \quad (8)$$

Once the induced electric dipoles are known [Eqs. (7) and (8)], the SHG signal for each direction can be calculated as³⁹

$$\begin{aligned} E_{2\omega,x}^{(X)}(r, \theta, \varphi) &= \left[\left(\sqrt{\frac{\pi}{2}} \right)^3 w_{xy}^2 w_z \right] N_v \frac{\eta}{r} \sqrt{\sin^2 \theta \sin^2 \varphi + \cos^2 \theta} \\ &\times \exp \left[-\frac{k_{2\omega}^2}{8} (w_{xy}^2 \sin^2 \theta + w_z^2 (\cos \theta - \xi')^2) \right] \\ &\times \left[\frac{1}{2} (E_{\omega,X}^{(0)})^2 (\beta_{xxx} \cos^2 \chi + \beta_{xyy} \sin^2 \chi) \right], \end{aligned} \quad (9)$$

$$\begin{aligned} E_{2\omega,y}^{(X)}(r, \theta, \varphi) &= \left[\left(\sqrt{\frac{\pi}{2}} \right)^3 w_{xy}^2 w_z \right] N_v \frac{\eta}{r} \sqrt{\sin^2 \theta \sin^2 \varphi + \cos^2 \theta} \\ &\times \exp \left[-\frac{k_{2\omega}^2}{8} (w_{xy}^2 \sin^2 \theta + w_z^2 (\cos \theta - \xi')^2) \right] \\ &\times \left[\frac{1}{2} (E_{\omega,X}^{(0)})^2 \beta_{xyy} \sin(2\chi) \right], \end{aligned} \quad (10)$$

related to the incident field $E_{\omega,X}$ and

$$\begin{aligned}
 E_{2\omega,x}^{(Y)}(r, \theta, \varphi) &= \left[\left(\sqrt{\frac{\pi}{2}} \right)^3 w_{xy}^2 w_z \right] N_v \frac{\eta}{r} \sqrt{\sin^2 \theta \sin^2 \varphi + \cos^2 \theta} \\
 &\times \exp \left[-\frac{k_{2\omega}^2}{8} (w_{xy}^2 \sin^2 \theta + w_z^2 (\cos \theta - \xi')^2) \right] \\
 &\times \left[\frac{1}{2} (E_{\omega,Y}^{(0)})^2 (\beta_{xxx} \sin^2 \chi + \beta_{xyy} \cos^2 \chi) \right] \exp[i2\delta], \quad (11)
 \end{aligned}$$

$$\begin{aligned}
 E_{2\omega,y}^{(Y)}(r, \theta, \varphi) &= - \left[\left(\sqrt{\frac{\pi}{2}} \right)^3 w_{xy}^2 w_z \right] N_v \frac{\eta}{r} \sqrt{\sin^2 \theta \sin^2 \varphi + \cos^2 \theta} \\
 &\times \exp \left[-\frac{k_{2\omega}^2}{8} (w_{xy}^2 \sin^2 \theta + w_z^2 (\cos \theta - \xi')^2) \right] \\
 &\times \left[\frac{1}{2} (E_{\omega,Y}^{(0)})^2 \beta_{xyy} \sin(2\chi) \right] \exp[i2\delta], \quad (12)
 \end{aligned}$$

for the SHG signal generated by the incident field $E_{\omega,Y}$. N_v is the dipole volume density, $\eta = \omega^2 / (\pi \epsilon_0 c^2)$, $k_{2\omega} = (2\pi n_{2\omega}) / \lambda_{2\omega}$ and $\xi' = \xi(n_\omega / n_{2\omega})$. Then the SHG signal along the x direction is obtained by adding Eqs. (9) and (11)

$$\begin{aligned}
 E_{2\omega,x}(r, \theta, \varphi) &= \left[\left(\sqrt{\frac{\pi}{2}} \right)^3 w_{xy}^2 w_z \right] N_v \frac{\eta}{r} \sqrt{\sin^2 \theta \sin^2 \varphi + \cos^2 \theta} \\
 &\times \exp \left[-\frac{k_{2\omega}^2}{8} (w_{xy}^2 \sin^2 \theta + w_z^2 (\cos \theta - \xi')^2) \right] \\
 &\times \frac{1}{2} \left\{ (E_{\omega,X}^{(0)})^2 (\beta_{xxx} \cos^2 \chi + \beta_{xyy} \sin^2 \chi) \right. \\
 &\left. + (E_{\omega,Y}^{(0)})^2 (\beta_{xxx} \sin^2 \chi + \beta_{xyy} \cos^2 \chi) \times \exp[i2\delta] \right\}. \quad (13)
 \end{aligned}$$

Similarly, adding Eqs. (10) and (12) we find the following expression for the SHG signal in the y direction

$$\begin{aligned}
 E_{2\omega,y}(r, \theta, \varphi) &= \left[\left(\sqrt{\frac{\pi}{2}} \right)^3 w_{xy}^2 w_z \right] N_v \frac{\eta}{r} \sqrt{\sin^2 \theta \sin^2 \varphi + \cos^2 \theta} \\
 &\times \exp \left[-\frac{k_{2\omega}^2}{8} (w_{xy}^2 \sin^2 \theta + w_z^2 (\cos \theta - \xi')^2) \right] \\
 &\times \frac{1}{2} \left\{ (E_{\omega,X}^{(0)})^2 \beta_{xyy} \sin(2\chi) \right. \\
 &\left. - (E_{\omega,Y}^{(0)})^2 \beta_{xyy} \sin(2\chi) \times \exp[i2\delta] \right\}. \quad (14)
 \end{aligned}$$

Provided that, in our case, the phase shift $\delta = \pm\pi/2$ and that it is related to the azimuth and ellipticity by

$$\tan \delta = \frac{\tan(2\psi)}{\sin(2\chi)}. \quad (15)$$

Phase shift δ is defined positive when $2\chi = 0$ and the ellipticity ranges between $0 < 2\psi < \pi/2$, which corresponds to the north hemisphere of the Poincaré sphere. On the other hand, δ is defined as negative when azimuth $2\chi = \pi$ and $-\pi/2 < 2\psi < 0$, so the ellipticity coordinate is located at the south hemisphere of the sphere.

From Fig. 1, the orthogonal fields $E_{\omega,XY}^{(0)}$ can be related to $E_{\omega}^{(0)}$ through ellipticity ψ

$$E_{\omega,x}^{(0)} = E_{\omega}^{(0)} \cos \psi \quad E_{\omega,y}^{(0)} = E_{\omega}^{(0)} \sin \psi, \quad (16)$$

and the SHG intensity along the x direction can be calculated by multiplying Eq. (13) by its complex conjugate and the expression $(1/2)n_{2\omega}\epsilon_0 c$

$$\begin{aligned}
 I_{2\omega,x}(r, \theta, \varphi) &= (E_{\omega}^{(0)})^4 \left[\frac{1}{8} n_{2\omega} \epsilon_0 c (N_v V)^2 \right] \left(\frac{\eta}{r} \right)^2 \\
 &\times (\sin^2 \theta \sin^2 \varphi + \cos^2 \theta) \\
 &\times \exp \left[-\frac{k_{2\omega}^2}{4} (w_{xy}^2 \sin^2 \theta + w_z^2 (\cos \theta - \xi')^2) \right] \\
 &\times [\cos^4 \psi (\beta_{xxx} \cos^2 \chi + \beta_{xyy} \sin^2 \chi)^2 \\
 &+ \sin^4 \psi (\beta_{xxx} \sin^2 \chi + \beta_{xyy} \cos^2 \chi)^2 \\
 &+ \frac{1}{2} \sin^2(2\psi) (\beta_{xxx} \cos^2 \chi + \beta_{xyy} \sin^2 \chi) \\
 &\times (\beta_{xxx} \sin^2 \chi + \beta_{xyy} \cos^2 \chi) \cos(2\delta)], \quad (17)
 \end{aligned}$$

where $V = (\sqrt{\pi/2})^2 w_{xy}^2 w_z$ is the active SHG volume. Similarly, the SHG intensity along the y direction can be written as

$$\begin{aligned}
 I_{2\omega,y}(r, \theta, \varphi) &= (E_{\omega}^{(0)})^4 \left[\frac{1}{8} n_{2\omega} \epsilon_0 c (N_v V)^2 \right] \left(\frac{\eta}{r} \right)^2 \\
 &\times (\sin^2 \theta \sin^2 \varphi + \cos^2 \theta) \\
 &\times \exp \left[-\frac{k_{2\omega}^2}{4} (w_{xy}^2 \sin^2 \theta + w_z^2 (\cos \theta - \xi')^2) \right] \\
 &\times \beta_{xyy}^2 \sin^2(2\chi) [\cos^4 \psi + \sin^4 \psi \\
 &- \frac{1}{2} \sin^2(2\psi) \cos(2\delta)]. \quad (18)
 \end{aligned}$$

The total SHG intensity is obtained by adding Eqs. (17) and (18). Since the incident beam intensity on the collagen fiber is given by $I_w = (1/2)n_\omega\epsilon_0 c |E_{\omega}^{(0)}|^2$, the final expression for SHG intensity as a function of the incoming polarization state (expressed in 2χ and 2ψ coordinates) and spherical coordinates (r , θ , and φ) can be written as

$$\begin{aligned}
 I_{2\omega}(\chi, \psi, r, \theta, \varphi) &= \left[\frac{I_w^2}{2} \frac{n_{2\omega}}{n_\omega^2 \epsilon_0 c} (N_v V)^2 \right] \left(\frac{\eta}{r} \right)^2 \\
 &\times (\sin^2 \theta \sin^2 \varphi + \cos^2 \theta) \\
 &\times \exp \left[-\frac{k_{2\omega}^2}{4} (w_{xy}^2 \sin^2 \theta + w_z^2 (\cos \theta - \xi')^2) \right] \\
 &\times [\cos^4 \psi ((\beta_{xxx} \cos^2 \chi + \beta_{xyy} \sin^2 \chi)^2 + \beta_{xyy}^2 \sin^2(2\chi)) \\
 &+ \sin^4 \psi ((\beta_{xxx} \sin^2 \chi + \beta_{xyy} \cos^2 \chi)^2 + \beta_{xyy}^2 \sin^2(2\chi)) \\
 &+ \frac{1}{2} \sin^2(2\psi) \cos(2\delta) ((\beta_{xxx} \cos^2 \chi + \beta_{xyy} \sin^2 \chi) \\
 &\times (\beta_{xxx} \sin^2 \chi + \beta_{xyy} \cos^2 \chi) - \beta_{xyy}^2 \sin^2(2\chi))]. \quad (19)
 \end{aligned}$$

References

1. A. Rich and F. H. C. Crick, "Molecular structure of collagen," *J. Mol. Biol.* 3(5), 483–506 (1961).

2. D. R. Keene, L. Y. Sakai, and R. E. Burgeson, "Human bone contains type-III collagen, type-VI collagen, and fibrillin: type-III collagen is present on specific fibers that may mediate attachment of tendons, ligaments, and periosteum to calcified bone cortex," *J. Histochem. Cytochem.* **39**(1), 59–69 (1991).
3. D. J. Hulmes, "Building collagen molecules, fibrils and suprafibrillar structures," *J. Struct. Biol.* **137**(1–2), 2–10 (2002).
4. M. D. Shoulders and R. T. Raines, "Collagen structure and stability," *Annu. Rev. Biochem.* **78**, 929–58 (2009).
5. J. M. Bueno, E. J. Gualda, and P. Artal, "Analysis of corneal stroma organization with wavefront optimized nonlinear microscopy," *Cornea* **30**(6), 692–701 (2011).
6. B. Fuentes et al., "Progressive extracellular matrix disorganization in chemically induced murine oral squamous cell carcinoma," *ISRN Pathol.* (2012).
7. Y. Guo et al., "Second harmonic tomography of tissues," *Opt. Lett.* **22**(17), 1323–1325 (1997).
8. P. J. Campagnola et al., "Second-harmonic imaging microscopy of living cells," *J. Biomed. Opt.* **6**(3), 277–286 (2001).
9. P. J. Campagnola et al., "High-resolution nonlinear optical imaging of live cells by second harmonic generation," *Biophys. J.* **77**(6), 3341–3349 (1999).
10. R. M. Williams, W. R. Zipfel, and W. W. Webb, "Interpreting second-harmonic generation images of collagen I fibrils," *Biophys. J.* **88**(2), 1377–1386 (2005).
11. A. Erikson et al., "Quantification of the second-order nonlinear susceptibility of collagen I using a laser scanning microscope," *J. Biomed. Opt.* **12**(4), 044002 (2007).
12. N. Morishige et al., "Second-harmonic imaging microscopy of normal human and keratoconus cornea," *Invest. Ophthalmol. Vision Sci.* **48**(3), 1087–1094 (2007).
13. N. Morishige et al., "Abnormalities of stromal structure in the bullous keratopathy cornea identified by second harmonic generation imaging microscopy," *Invest. Ophthalmol. Vision Sci.* **53**(8), 4998–5003 (2012).
14. J. M. Bueno et al., "Multiphoton microscopy of ex-vivo corneas after collagen cross-linking," *Invest. Ophthalmol. Vision Sci.* **52**(8), 5325–5331 (2011).
15. E. J. Gualda et al., "Femtosecond infrared intrastromal ablation and backscattering-mode adaptive-optics multiphoton microscopy in chicken corneas," *Biomed. Opt. Express* **2**(11), 2950–2960 (2011).
16. P. Stoller et al., "Quantitative second-harmonic generation microscopy in collagen," *Appl. Opt.* **42**(25), 5209–5219 (2003).
17. J. Duboisset et al., "Generic model of the molecular orientational distribution probed by polarization-resolved second-harmonic generation," *Phys. Rev. A* **85**(4), 43829 (2012).
18. K. Tilbury et al., "Differentiation of col I and col III isoforms in stromal models of ovarian cancer by analysis of second harmonic generation polarization and emission directionality," *Biophys. J.* **106**(2), 354–365 (2014).
19. I. Gusachenko et al., "Polarization-resolved second harmonic microscopy in anisotropic thick tissues," *Opt. Express* **18**(18), 19339–19352 (2010).
20. S. Roth and I. Freund, "Second harmonic generation in collagen," *J. Chem. Phys.* **70**(4), 1637–1643 (1979).
21. Y. Chang et al., "Theoretical simulation study of linearly polarized light on microscopic second-harmonic generation in collagen type I," *J. Biomed. Opt.* **14**(4), 044016 (2009).
22. C. Odin et al., "Orientation fields of nonlinear biological fibrils by second harmonic generation microscopy," *J. Microsc.* **229**(1), 32–38 (2008).
23. I. Freund, M. Deutsch, and A. Sprecher, "Connective tissue polarity. Optical second-harmonic microscopy, crossed-beam summation, and small-angle scattering in rat-tail tendon," *Biophys. J.* **50**(4), 693–712 (1986).
24. P. Stoller et al., "Polarization-dependent optical second-harmonic imaging of a rat-tail tendon," *J. Biomed. Opt.* **7**(2), 205–214 (2002).
25. F. Tiaho, F. G. Recher, and D. Roue, "Estimation of helical angles of myosin and collagen by second harmonic generation imaging microscopy," *Opt. Express* **15**(19), 12286–12295 (2007).
26. R. M. Plocinik et al., "Modular ellipsometric approach for mining structural information from nonlinear optical polarization analysis," *Phys. Rev. B* **72**(12), 125409 (2005).
27. O. del Barco and J. M. Bueno, "Second harmonic generation signal in collagen fibers: role of polarization, numerical aperture, and wavelength," *J. Biomed. Opt.* **17**(4), 045005 (2012).
28. I. J. Su et al., "Determination of collagen nanostructure from second-order susceptibility tensor analysis," *Biophys. J.* **100**(8), 2053–2062 (2011).
29. A. E. Tuer et al., "Nonlinear optical properties of type I collagen fibers studied by polarization dependent second harmonic generation microscopy," *J. Phys. Chem. B* **115**(44), 12759–12769 (2011).
30. P. J. Su et al., "Discrimination of collagen in normal and pathological skin dermis through second-order susceptibility microscopy," *Opt. Express* **17**(13), 11161–11171 (2009).
31. X. Chen, C. Raggio, and P. J. Campagnola, "Second-harmonic generation circular dichroism studies of osteogenesis imperfecta," *Opt. Lett.* **37**(18), 3837–3839 (2012).
32. A. Golaraei et al., "Characterization of collagen in non-small cell lung carcinoma with second harmonic polarization microscopy," *Biomed. Opt. Express* **5**(10), 3562–3567 (2014).
33. W. R. Zipfel, R. M. Williams, and W. W. Webb, "Nonlinear magic: multiphoton microscopy in the biosciences," *Nat. Biotechnol.* **21**(11), 1369–1377 (2003).
34. H. G. Jerrard, "Quarter-wave compensator with a sensitive half-shadow device," *J. Opt. Soc. Am.* **44**(4), 289–296 (1954).
35. V. Le Floch et al., "Monitoring of orientation in molecular ensembles by polarization sensitive nonlinear microscopy," *J. Phys. Chem. B* **107**(45), 12403–12410 (2003).
36. S. Brasselet, "Polarization-resolved nonlinear microscopy: application to structural molecular and biological imaging," *Adv. Opt. Photonics* **3**, 205–271 (2011).
37. J. M. Bueno, "Measurement of parameters of polarization in the living human eye using imaging polarimetry," *Vision Res.* **40**(28), 3791–3799 (2000).
38. G. Hall et al., "Experimental and simulation study of the wavelength dependent second harmonic generation of collagen in scattering tissues," *Opt. Lett.* **39**(7), 1897–1900 (2014).
39. J. Bigun and G. H. Granlund, "Optimal orientation detection of linear symmetry," in *First Int. Conf. on Computer Vision, ICCV, London, June 8–11*, pp 433–438, IEEE Computer Society (1987).
40. B. Jahne, *"Spatio-Temporal Image Processing: Theory and Scientific Applications,"* Springer, Berlin (1993).
41. D. Marsh, "Dichroic ratios in polarized Fourier transform infrared for non axial symmetry of β -sheet structures," *Biophys. J.* **72**(6), 2710–2718 (1997).
42. A. Zoumi, Y. Alvin, and B. J. Tromberg, "Imaging cells and extracellular matrix in vivo by using second-harmonic generation and two-photon excited fluorescence," *PNAS* **99**(17), 11014–11019 (2002).
43. P. Stoller et al., "Polarization-modulated second harmonic generation in collagen," *Biophys. J.* **82**(6), 3330–3342 (2002).
44. L. Moreaux et al., "Coherent scattering in multi-harmonic light microscopy," *Biophys. J.* **80**(3), 1568–1574 (2001).
45. A. Willetts, J. E. Rice, and D. M. Burland, "Problems in the comparison of theoretical and experimental hyperpolarizabilities," *J. Chem. Phys.* **97**(10), 7590 (1992).
46. R. W. Boyd, *Nonlinear Optics*, Academic Press, San Diego (1992).

Biographies for the authors are not available.